Molecular spintronics: Coherent spin transfer in coupled quantum dots

Florian Meier,[1,2,*] Veronica Cerletti,[2] Oliver Gywat,[2] Daniel Loss,[2] and D. D. Awschalom[1,3]
[1]*California Nanosystems Institute, University of California, Santa Barbara, California 93106, USA*
[2]*Department of Physics and Astronomy, University of Basel, Klingelbergstrasse 82, 4056 Basel, Switzerland*
[3]*Department of Physics, University of California, Santa Barbara, California 93106, USA*
(Received 21 January 2004; published 26 May 2004)

Time-resolved Faraday rotation has recently demonstrated coherent transfer of electron spin between quantum dots coupled by conjugated molecules. Using a transfer Hamiltonian ansatz for the coupled quantum dots, we calculate the Faraday rotation signal as a function of the probe frequency in a pump-probe setup using neutral quantum dots. Additionally, we study the signal of one spin-polarized excess electron in the coupled dots. We show that, in both cases, the Faraday rotation angle is determined by the spin transfer probabilities and the Heisenberg spin-exchange energy. By comparison of our results with experimental data, we find that the transfer matrix element for electrons in the conduction band is of order 0.08 eV and the spin transfer probabilities are of order 10%.

DOI: 10.1103/PhysRevB.69.195315 PACS number(s): 78.67.Hc, 85.65.+h, 85.75.−d

I. INTRODUCTION

The past years have evidenced rapid experimental progress in the field of spintronics.[1,2] Coherent transport of electron spins in semiconductors has been demonstrated over several micrometers,[3] nourishing hopes that the electron spin may be used as carrier of information similar to the electron charge. Such applications of the spin degree of freedom for classical or quantum information processing[4] require control of the electron spin not only in extended systems such as two-dimensional electron gases (2DEG's), but rather also for spins localized in quantum dots (QD's).

Recently, coherent transfer of electron spin has been observed between QD's with different radii $r_A \simeq 1.7$ nm (QD A) and $r_B \simeq 3.5$ nm (QD B) coupled by a benzene ring.[5] The different QD radii give rise to different quantum size levels for electrons and holes in the two species of QD's. The resulting difference in exciton energies allows one to pump and probe selectively the spin polarization for QD's of species A and B. The main result of Ref. 5 is that an electron spin polarization created by optical pumping in QD B is transferred ''instantaneously'' to QD A. The efficiency of this transfer mechanism is of order 10% at low temperatures $T < 50$ K and increases to approximately 20% for $T \gtrsim 100$ K. The observed shift of the exciton energies to lower values compared to isolated QD's is also consistent with a coherent delocalization of the electron or hole over the system formed by the QD's and the bridging molecule.

The purpose of this paper is to show that a two-site Hamiltonian with a transfer term captures some of the essential experimental features. We aim at calculating the dependence of the experimentally observed Faraday rotation (FR) signal as a function of probe energy on microscopic parameters such as spin transfer probabilities. The FR angle is proportional to the difference in refractive indices for $\sigma^{\pm}$ circularly polarized light which is determined by the difference of the dielectric response functions. We calculate the dielectric response functions of coupled QD's and derive an analytical expression for the FR angle in terms of electron transfer probabilities and Heisenberg exchange splittings. The experimental data provide strong evidence that the spin transfer is mediated by the π-conjugated molecule.[6] We do not aim to describe this transfer mechanism microscopically, but consider the transfer matrix elements for electrons and holes as parameters of the Hamiltonian.

For CdSe QD's with radii r_A and r_B, the single-particle level spacing for electrons and holes is large compared to the temperatures $T \leqslant 200$ K explored experimentally. This allows us to restrict our attention to the lowest orbital levels in the conduction and valence band of both QD's. A possible admixing of higher orbital levels caused by the Coulomb interaction is determined by the parameter $r_{A,B}/a_X$, where $a_X \simeq 5.4$ nm is the exciton radius for CdSe.[7] For the small QD's in Ref. 5, the Coulomb interaction is small compared to the single-particle level spacing, such that the admixing of higher orbital levels to the ground state is small as well. (For details on experimental parameters, see Sec. V.) This allows us to describe the coupled QD's by the Hamiltonian

$$\hat{H} = \hat{H}_0 + \hat{H}_{\mathrm{Coul}} + \hat{H}_T, \tag{1}$$

where

$$\hat{H}_0 = \sum_{\nu=A,B;\sigma=\pm} (E_c^{\nu} \hat{c}_{c,\sigma}^{\nu\dagger} \hat{c}_{c,\sigma}^{\nu} + E_v^{\nu} \hat{c}_{v,\sigma}^{\nu\dagger} \hat{c}_{v,\sigma}^{\nu}) \tag{2}$$

contains the single-particle levels of uncoupled QD's $\nu = A,B$. The operators $\hat{c}_c^{\nu,\sigma}$ and $\hat{c}_v^{\nu,\sigma}$ annihilate an electron in the lowest level E_c^{ν} of the conduction band with spin quantum number $s_z = \sigma 1/2$ and the highest level in the valence band E_v^{ν}, with angular momentum $j_z = \sigma 3/2$, respectively, where $\sigma = \pm$. Here, we have adopted a simple model for the change in the band structure of CdSe due to the QD confinement. We assume a spherical QD shape and a splitting of the $j = 3/2$ valence band at the Γ point into the heavy hole (hh) and light hole (lh) subband with total angular momentum projection $j_z = \pm 3/2$ and $j_z = \pm 1/2$, respectively, as obtained, e.g., from the Luttinger Hamiltonian with an additional anisotropy term for the crystal field of the hexagonal lattice.[8]

 ©2004 The American Physical Society

The lh subband will therefore be neglected in the following. The Coulomb interaction energy is

$$\hat{H}_{\mathrm{Coul}}=\sum_{\nu=A,B}\frac{U_\nu}{2}[\hat{n}_c^\nu(\hat{n}_c^\nu-1)+\hat{n}_v^\nu(\hat{n}_v^\nu-1)-2\hat{n}_c^\nu\hat{n}_v^\nu], \quad (3)$$

where $\hat{n}_c^\nu=\Sigma_{\sigma=\pm}\hat{c}_{c,\sigma}^{\nu\dagger}\hat{c}_{c,\sigma}^{\nu}$ and $\hat{n}_v^\nu=\Sigma_{\sigma=\pm}\hat{c}_{v,\sigma}^{\nu}\hat{c}_{v,\sigma}^{\nu\dagger}$ are the number operators for electrons in the conduction-band level and holes in the valence-band level. $U_\nu\simeq e^2/4\pi\epsilon\epsilon_0 r_\nu$ is the characteristic charging energy of QD A and B, respectively. Transfer of spin and charge between the QD's is accounted for by the transfer Hamiltonian

$$\hat{H}_T=\sum_{\sigma=\pm}(t_c\hat{c}_{c,\sigma}^{A\dagger}\hat{c}_{c,\sigma}^{B}+t_v\hat{c}_{v,\sigma}^{A\dagger}\hat{c}_{v,\sigma}^{B}+\mathrm{H.c.}), \quad (4)$$

where we assume that transfer of electrons through the π-conjugated molecule conserves the electron spin both in the conduction and the valence band.

The ansatz for the Hamiltonian in Eqs. (1)–(4) is a model in which the biexciton shift, the exciton fine structure, and the electrostatic coupling between the QD's have been neglected. We will justify this in Sec. V below where we discuss our results for the experimental parameters of Ref. 5. Because the focus of this work is to calculate the FR angle that results from transfer of electrons between the QD's, we assume for simplicity that the symmetry axis of the QD's with hexagonal crystal structure is parallel to the direction of pump and probe laser pulses. The effect of a random QD orientation will be discussed in Sec. V.

In the following, we analyze the results of Ref. 5 based on the Hamiltonian Eq. (1). This paper is organized as follows. In Sec. II, we calculate the time-resolved FR signal for an electron wave function which is delocalized over QD's A and B. In Sec. III, we calculate the FR angle as a function of probe energy for an initial spin polarization created by optical pumping. We take into account both electron transfer processes and the Coulomb interaction and show that these terms give rise to an exchange splitting of the two-exciton eigenstates. In Sec. IV, we perform the related analysis for a system with one spin-polarized excess electron in the QD's. In Sec. V, we discuss our results for the parameters of CdSe QD's coupled by benzene molecules,[5] calculate the transfer matrix element and spin transfer probabilities. In Sec. VI, we draw our conclusions.

II. TIME-RESOLVED FARADAY ROTATION FOR COUPLED QUANTUM DOTS

Before we calculate the FR angle for the general Hamiltonian, Eq. (1), in Secs. III and IV below, we first consider time-resolved FR for a particularly simple case in which a single electron is in a coherent superposition of states in QD's A and B at time $t=0$, $|\psi(0)\rangle=(\hat{c}_{c,+}^{B\dagger}+\alpha\hat{c}_{c,+}^{A\dagger})|0\rangle/\sqrt{1+\alpha^2}$. We further assume $t_{c,v}=0$ and $E_c^A=E_c^B$ in Eq. (1) for $t>0$. Here, $|0\rangle$ denotes the vacuum state in which the valence band in both QD's is filled and the conduction-band states are empty. This simple scenario, although unrealistic because transfer matrix elements are assumed to vanish after the initial state $|\psi_0\rangle$ has been prepared, will allow us to derive simple analytical expressions for the FR angle even in presence of a magnetic field. The simplifying assumptions $t_{c,v}=0$ and $E_c^A=E_c^B$ will be lifted in the microscopic discussion in Secs. III and IV.

The different radii r_A and r_B of the CdSe QD's lead to different g factors and different Larmor precession frequencies $\omega_\nu=g_\nu\mu_B B_{ext}/\hbar$,[9–11] where B_{ext} is an external magnetic field perpendicular to the spin quantization axis which is given by the symmetry axis of the CdSe QD's, and g_ν are the electron g factors for $\nu=A,B$. At time t,

$$|\psi(t)\rangle=\frac{1}{\sqrt{1+\alpha^2}}[\cos(\omega_B t/2)\hat{c}_{c,+}^{B\dagger}-i\sin(\omega_B t/2)\hat{c}_{c,-}^{B\dagger}+\alpha\cos(\omega_A t/2)\hat{c}_{c,+}^{A\dagger}-i\alpha\sin(\omega_A t/2)\hat{c}_{c,-}^{A\dagger}]|0\rangle. \quad (5)$$

This time evolution of the electron spin can be detected by FR because the FR angle θ_F is determined by the population imbalance between the $s_z=\pm 1/2$ conduction-band states in this situation.[12–14] For probe pulse frequency E/h, θ_F is proportional to the difference of the real parts of the dielectric response functions $\epsilon(E)$ for $\sigma^\pm$ circularly polarized light.[12] With the spectral representation of the response functions, $\theta_F(E)$ is expressed in terms of the transition-matrix elements between the state $|\psi(t)\rangle$ with energy E_0 and all intermediate states $|\psi_i\rangle$ which are virtually excited by the probe pulse,

$$\theta_F(E,t)=CE\sum_{|\psi_i\rangle}\frac{E-(E_i-E_0)}{[E-(E_i-E_0)]^2+\Gamma^2}(|\langle\psi_i|\hat{P}_+|\psi(t)\rangle|^2-|\langle\psi_i|\hat{P}_-|\psi(t)\rangle|^2). \quad (6)$$

The polarization operators $\hat{P}_\pm=d_A\hat{c}_{c,\pm}^{A\dagger}\hat{c}_{v,\pm}^{A}+d_B\hat{c}_{c,\pm}^{B\dagger}\hat{c}_{v,\pm}^{B}$ couple to the $\sigma^\mp$ circularly polarized components of the probe pulse. d_ν are the dipole transition matrix elements for transition from the $j_z=\pm 3/2$ valence-band states to the $s_z=\pm 1/2$ conduction-band states in QD's A and B. $E_0=E_c^B$ and E_i are the energy eigenvalues of the initial state and the intermediate state $|\psi_i\rangle$, respectively, and the level broadening Γ accounts for a finite lifetime of the orbital levels. The prefactor $C\propto L/(hcn_0)$ is determined by the size L of the sample and the refraction index n_0 of bulk CdSe.

Because we have assumed an initial state $|\psi(0)\rangle$ with one electron, all intermediate states $|\psi_i\rangle$ in Eq. (6) are energy eigenstates with two electrons and one hole. For $t_{c,v}=0$ in Eq. (1), these are of the form $|\psi_i\rangle=\hat{c}_{c,\sigma}^{\nu\dagger}\hat{c}_{v,\sigma}^{\nu}\hat{c}_{c,\sigma'}^{\nu'\dagger}|0\rangle$ with $\sigma,\sigma'=\pm$ and $\nu,\nu'=A,B$. Pauli blocking prohibits the creation of an exciton with electron spin $\sigma 1/2$ if the conduction-band level is already occupied by an electron with the same spin. The resulting difference in transition matrix elements for $\hat{P}_+$ and $\hat{P}_-$ is proportional to the population imbalance of the $s_z=\pm 1/2$ levels. For a probe pulse at time t, from Eq. (6) we obtain directly

$$\theta_F(E,t)=\frac{CE}{1+\alpha^2}\left[d_B^2\frac{E-E_X^B}{(E-E_X^B)^2+\Gamma^2}\cos(\omega_B t)+\alpha^2 d_A^2\frac{E-E_X^A}{(E-E_X^A)^2+\Gamma^2}\cos(\omega_A t)\right], \quad (7)$$

where $E_X^\nu=E_c^\nu-E_v^\nu-U_\nu$ is the exciton energy for QD ν.

$\theta_F(E,t)$ shows coherent oscillations with frequencies ω_A and ω_B caused by the electron spin precessing around the external magnetic field. In reality, these coherent oscillations are exponentially damped with a spin dephasing rate Γ_S which is typically much smaller than the orbital dephasing rate, $\Gamma_S \ll \Gamma$. Taking into account spin dephasing, the Fourier transform of the time-resolved FR signal as a function of the probe pulse energy E and the Fourier frequency ω is

$$\theta_F(E,\omega)=\frac{CE}{1+\alpha^2}\left[d_B^2\frac{E-E_X^B}{(E-E_X^B)^2+\Gamma^2}\frac{\Gamma_S}{(\omega-\omega_B)^2+\Gamma_S^2}+\alpha^2 d_A^2\frac{E-E_X^A}{(E-E_X^A)^2+\Gamma^2}\frac{\Gamma_S}{(\omega-\omega_A)^2+\Gamma_S^2}\right]. \quad (8)$$

$\theta_F(E,\omega)$ shows characteristic features for $E\simeq E_X^\nu$ and $\omega\simeq\omega_\nu$. The two terms in Eq. (8) describe the dielectric response due to virtual creation of an exciton in QD A and B, respectively. For $E_X^B \lesssim E \lesssim E_X^A$, they have different sign and may cancel. Figure 1(a) shows a gray scale plot of $|\theta_F(E,\omega)|$ for the experimental values $E_X^B=2.06$ eV, $E_X^A=2.41$ eV, $\Gamma=0.05$ eV, and $\Gamma_S/2\pi=0.5$ GHz, assuming $d_A^2/d_B^2=1$ and $\alpha^2=0.2$. For Fig. 1(b), $\Gamma=0.035$ eV, and $\Gamma_S/2\pi=1.2$ GHz, and $\alpha^2=0.4$. One of the most characteristic features of the experimental data [Fig. 2(c) in Ref. 5] is that $|\theta_F(E,\omega)|$ vanishes and reappears as a function of probe pulse frequency E for $\omega\simeq\omega_B$. This feature is also present in the theoretical result and can be traced back to the superposition of two response functions in Eq. (8). More specifically, for $\omega\simeq\omega_B$ and $E\simeq E_X^A-\Gamma$, the two terms in Eq. (8) have opposite sign and cancel for sufficiently large α.

Above, we have assumed that the electron delocalized over both QD's at $t=0$ retains spatial coherence. For rapid decoherence of the orbital part of the wave function, the initial state is described by the density matrix $\hat{\rho}=(\hat{c}_{c,+}^{B\dagger}|0\rangle\times\langle 0|\hat{c}_{c,+}^{B}+\alpha^2\hat{c}_{c,+}^{A\dagger}|0\rangle\langle 0|\hat{c}_{c,+}^{A})/(1+\alpha^2)$. The FR signal in this case is the incoherent superposition of the FR signals for QD A and B, and is identical to the results in Eqs. (7) and (8). Hence, a FR signal as shown in Fig. 1 does not allow one to distinguish coherent from incoherent spatial superpositions.

III. OPTICAL SPIN INJECTION

In the preceding section, $\theta_F(E)$ was calculated for the simple case of a single electron delocalized over the coupled QD's. So far, we have also neglected that all intermediate states $|\psi_i\rangle$ in Eq. (6) that are virtually excited by the probe pulse will be modified by finite transfer energies $t_{c,v}$. We next turn to a microscopic analysis in which we take into account $t_{c,v}\neq 0$ also for the intermediate states.

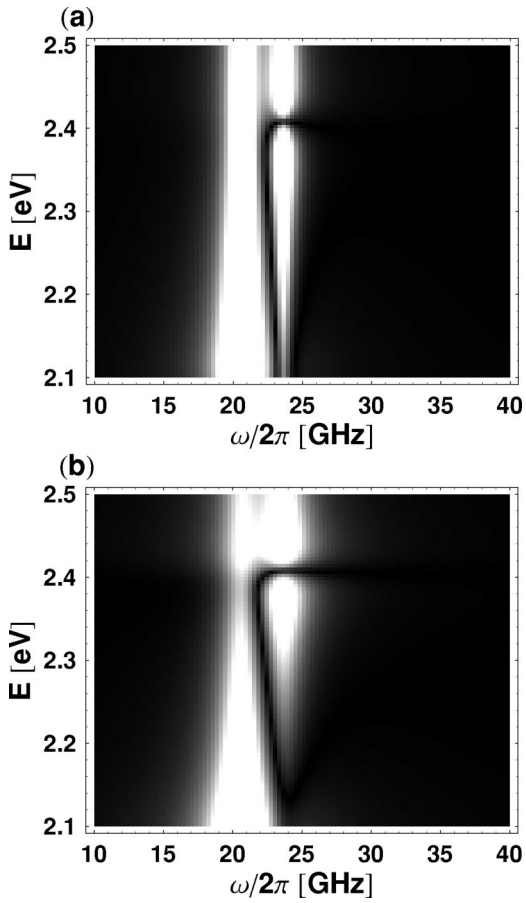

FIG. 1. (a) Gray scale plot of the FR angle $|\theta_F|$ [given in Eq. (8)] in arbitrary units as function of probe pulse frequency E/h and frequency $f=\omega/2\pi$. We have chosen the parameters[5] $E_X^A=2.41$ eV, $E_X^B=2.06$ eV, $\omega_A/2\pi=23.6$ GHz, $\omega_B/2\pi=20.6$ GHz, $\Gamma=0.05$ eV, $\Gamma_S/2\pi=0.5$ GHz, and $\alpha^2=0.2$. (b) For $\Gamma=0.035$ eV, $\Gamma_S/2\pi=1.2$ GHz, and $\alpha^2=0.4$, pronounced features caused by the interplay of the two terms in Eq. (8) become more clearly visible. In particular, the FR signal at $\omega\simeq\omega_B$ vanishes and reappears as a function of probe pulse frequency E.

In Ref. 5, the initial state prepared by optical pumping is a one-exciton state. Similar to the analysis in Sec. II above, the FR angle as a function of probe energy is proportional to the difference of the dielectric response functions for $\sigma^\pm$ circularly polarized light [Eq. (6)]. In order to evaluate this expression, both the initial one-exciton state and all intermediate two-exciton states which are virtually excited by the probe pulse must be calculated for the coupled QD's. In this section, we first calculate the one-exciton energy eigenstate of the coupled QD's prepared by the pump pulse and subsequently identify all two-exciton eigenstates $|\psi_i\rangle$ which are virtually excited by the probe pulse. Our analysis is based on perturbation theory in the transfer energies and is valid if $|t_{c,v}|$ is the smallest energy scale, $|t_{c,v}| \ll \delta E_c, |\delta E_v|, U_A, U_B, |\delta E_{c,v}\pm U_{A,B}|$. Here, we have defined the energy differences $\delta E_c=E_c^A-E_c^B\geq 0$ and $\delta E_v=E_v^A-E_v^B\leq 0$ between the conduction-band and valence-band levels of QD's A and B.

In Ref. 5, an initial spin polarization was created by optical pumping. For $t_{c,v}=0$, the states $\hat{c}^{\nu\dagger}_{c,\sigma}\hat{c}^{\nu}_{v,\sigma}|0\rangle$ are one-exciton eigenstates with energy eigenvalues

$$E_X^{\nu(0)}=E_c^{\nu}-E_v^{\nu}-U_{\nu}, \tag{9}$$

which are prepared by absorption of a $-\sigma$ circularly polarized pump pulse. To first order in the transfer energies $t_{c,v}$, the energy eigenstates are

$$|X_{A,\sigma}\rangle=\hat{c}^{A\dagger}_{c,\sigma}\hat{c}^{A}_{v,\sigma}|0\rangle+\left(\frac{t_c}{\delta E_c-U_A}\hat{c}^{B\dagger}_{c,\sigma}\hat{c}^{A}_{v,\sigma}+\frac{t_v}{\delta E_v+U_A}\hat{c}^{A\dagger}_{c,\sigma}\hat{c}^{B}_{v,\sigma}\right)|0\rangle, \tag{10a}$$

$$|X_{B,\sigma}\rangle=\hat{c}^{B\dagger}_{c,\sigma}\hat{c}^{B}_{v,\sigma}|0\rangle+\left(-\frac{t_c}{\delta E_c+U_B}\hat{c}^{A\dagger}_{c,\sigma}\hat{c}^{B}_{v,\sigma}-\frac{t_v}{\delta E_v-U_B}\hat{c}^{B\dagger}_{c,\sigma}\hat{c}^{A}_{v,\sigma}\right)|0\rangle, \tag{10b}$$

with eigenenergies

$$E_X^{A}=E_X^{A(0)}+\frac{t_c^2}{\delta E_c-U_A}-\frac{t_v^2}{\delta E_v+U_A}, \tag{11a}$$

$$E_X^{B}=E_X^{B(0)}-\frac{t_c^2}{\delta E_c+U_B}+\frac{t_v^2}{\delta E_v-U_B}. \tag{11b}$$

As expected, the eigenenergies are shifted due to the delocalization of electrons and holes over the coupled QD's. The exciton states in Eq. (10) are the only one-exciton states which can be prepared by the absorption of a photon with circular polarization $-\sigma$ if the photon is incident along the hexagonal axis of the CdSe crystal structure. However, a photon with energy $E\simeq E_X^B$ no longer creates an exciton only in QD *B*, but an exciton in which electron and hole are delocalized over the coupled QD system. This delocalization of the quantum-mechanical wave function is consistent with the short time scale for spin transfer observed experimentally.[5]

We now turn to the calculation of the FR angle, assuming that the pump pulse has prepared an initial state $|\psi\rangle=|X_{B,+}\rangle$. The evaluation of the dielectric response function will require us to calculate all two-exciton states that are virtually excited by the probe pulse. Interesting features in the FR signal effected by spin transfer are of order $t_{c,v}^2$. In order to keep the following expressions simple, we assume that spin is transferred between the conduction-band states and set $t_v=0$. Then, only the seven states $|A_+B_+\rangle$, $|T_0\rangle$, $|S\rangle$, $|B_+B_-\rangle$, $|\tilde{T}_0\rangle$, $|\tilde{S}\rangle$, and $|\widetilde{B_+B_-}\rangle$ listed below and in Appendix A have finite matrix elements up to $\mathcal{O}(t_c^2)$ with $\hat{P}_{\pm}|X_{B,+}\rangle$. For $\delta E_v+U_A\neq 0$, only the eigenenergies of $|A_+B_+\rangle$, $|T_0\rangle$, and $|S\rangle$ are close to the excitation energy of a probe pulse with frequency $E/h\simeq E_X^A/h$. Hence, these states dominate the spectral representation in Eq. (6).[15]

The polarization operator $\hat{P}_+$ induces transitions from the initial state $|X_{B,+}\rangle$ to

$$|A_+B_+\rangle=\hat{c}^{A\dagger}_{c,+}\hat{c}^{B\dagger}_{c,+}\hat{c}^{A}_{v,+}\hat{c}^{B}_{v,+}|0\rangle, \tag{12}$$

with energy eigenvalue

$$E_{A_+B_+}=E_X^{A(0)}+E_X^{B(0)}. \tag{13}$$

The notation indicates that two electrons with the same spin $s_z=1/2$ occupy the conduction-band states in QD's *A* and *B*, respectively, and form a spin triplet state. $|A_+B_+\rangle$ is an exact eigenstate of the Hamiltonian even for $t_c\neq 0$ because transfer of the conduction-band electrons is blocked by Pauli's exclusion principle. The matrix element $\langle A_+B_+|\hat{P}_+|X_{B_+}\rangle$ is the only finite matrix element of the operator $\hat{P}_+$.

Finite matrix elements for $\hat{P}_-$ come from the states in which the electrons in the conduction-band level form a spin triplet and singlet, respectively,

$$|T_0\rangle=\frac{1}{\sqrt{2}}(\hat{c}^{A\dagger}_{c,-}\hat{c}^{B\dagger}_{c,+}+\hat{c}^{A\dagger}_{c,+}\hat{c}^{B\dagger}_{c,-})\hat{c}^{A}_{v,-}\hat{c}^{B}_{v,+}|0\rangle, \tag{14a}$$

$$|S\rangle\propto\frac{1}{\sqrt{2}}(\hat{c}^{A\dagger}_{c,-}\hat{c}^{B\dagger}_{c,+}-\hat{c}^{A\dagger}_{c,+}\hat{c}^{B\dagger}_{c,-})\hat{c}^{A}_{v,-}\hat{c}^{B}_{v,+}|0\rangle+\sqrt{2}\left(\frac{t_c}{\delta E_c+U_B}\hat{c}^{A\dagger}_{c,+}\hat{c}^{A\dagger}_{c,-}-\frac{t_c}{\delta E_c-U_A}\hat{c}^{B\dagger}_{c,+}\hat{c}^{B\dagger}_{c,-}\right)\hat{c}^{A}_{v,-}\hat{c}^{B}_{v,+}|0\rangle, \tag{14b}$$

and the holes with $j_z=-3/2$ and $j_z=+3/2$ are localized in QD's *A* and *B*, respectively. Note that the projection of the total conduction-band spin onto the spin quantization axis vanishes for the triplet state $|T_0\rangle$. The normalization constant for $|S\rangle$ is defined by $\langle S|S\rangle=1$. The eigenenergies

$$E_{T_0}=E_X^{A(0)}+E_X^{B(0)}, \tag{15a}$$

$$E_S=E_X^{A(0)}+E_X^{B(0)}+2t_c^2\left(\frac{1}{\delta E_c-U_A}-\frac{1}{\delta E_c+U_B}\right) \tag{15b}$$

show an energy offset which is caused by the interdot exchange coupling.[4,16] The energies of $|A_+B_+\rangle$ and $|T_0\rangle$ are not shifted by electron transfer because of Pauli blocking and destructive interference of transfer paths, respectively.

The state

$$|B_+B_-\rangle\propto\left[\hat{c}^{B\dagger}_{c,+}\hat{c}^{B\dagger}_{c,-}+\frac{t_c}{\delta E_c-U_A}(\hat{c}^{A\dagger}_{c,-}\hat{c}^{B\dagger}_{c,+}-\hat{c}^{A\dagger}_{c,+}\hat{c}^{B\dagger}_{c,-})+\frac{2t_c^2\hat{c}^{A\dagger}_{c,+}\hat{c}^{A\dagger}_{c,-}}{(\delta E_c-U_A)(2\delta E_c-U_A+U_B)}\right]\hat{c}^{A}_{v,-}\hat{c}^{B}_{v,+}|0\rangle, \tag{16}$$

with

$$E_{B_+B_-}=E_X^{B(0)}+E_c^B-E_v^A-2\frac{t_c^2}{\delta E_c-U_A} \tag{17}$$

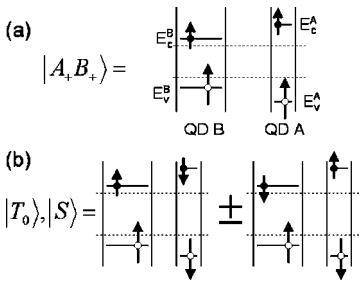

FIG. 2. Schematic representation of the spin configurations (in the electron picture) for states (a) $|A_+B_+\rangle$ and (b) $|S\rangle$, $|T_0\rangle$ to leading order in t_c. The dashed lines represent the conduction- and valence-band edge in bulk CdSe.

is offset in energy from $E_X^{A(0)}+E_X^{B(0)}$ even to zeroth order in t_c and does not contribute significantly to $\theta_F(E)$ for $E \simeq E_X^A$. The three states in Eqs. (14) and (16) provide the dominant terms in the spectral representation for θ_F in Eq. (6). In particular, they exhaust the sum rule $\Sigma_{|\psi_i\rangle}|\langle\psi_i|\hat{c}_{c,-}^{A\dagger}\hat{c}_{v,-}^{A}|X_{B,+}\rangle|^2=1$ up to $\mathcal{O}(t_c^2)$. In Fig. 2, the spin configurations for $|A_+B_+\rangle$, $|S\rangle$, and $|T_0\rangle$ are shown schematically.

From Eqs. (10b)–(17), the FR angle θ_F is readily evaluated. We denote the electron transfer probability from QD ν to QD ν' by $p_{\nu\to\nu'}$. We obtain

$$p_{A\to B}=\left(\frac{t_c}{\delta E_c-U_A}\right)^2, \tag{18a}$$

$$p_{B\to A}=\left(\frac{t_c}{\delta E_c+U_B}\right)^2. \tag{18b}$$

For the transition matrix elements of the dipole operators in Eq. (6), we obtain in terms of the transfer probabilities

$$|\langle A_+B_+|\hat{P}_+|X_{B,+}\rangle|^2=(1-p_{B\to A})d_A^2, \tag{19a}$$

$$|\langle T_0|\hat{P}_-|X_{B,+}\rangle|^2=\frac{1-p_{B\to A}}{2}d_A^2, \tag{19b}$$

$$|\langle S|\hat{P}_-|X_{B,+}\rangle|^2=\frac{1+p_{B\to A}-2p_{A\to B}}{2}d_A^2, \tag{19c}$$

$$|\langle B_+B_-|\hat{P}_-|X_{B,+}\rangle|^2=p_{A\to B}d_A^2. \tag{19d}$$

Because of the exchange splitting $E_{T_0}-E_S$ between conduction-band triplet and singlet states, finite transfer probabilities $p_{A\to B}$ and $p_{B\to A}$ lead to pronounced features in the FR angle as a function of the probe pulse frequency E/h. For probe energies $E_{T_0B}=E_{T_0}-E_X^B\leqslant E\leqslant E_{SB}=E_S-E_X^B$, the FR signal varies strongly with energy and is given by

$$\theta_F(E)=\frac{CEd_A^2}{2}\left[(1-p_{B\to A})\frac{E-E_{T_0B}}{(E-E_{T_0B})^2+\Gamma^2}\right.$$
$$\left.-(1+p_{B\to A}-2p_{A\to B})\frac{E-E_{SB}}{(E-E_{SB})^2+\Gamma^2}\right]. \tag{20}$$

For $|E-E_{SB}|\gtrsim|E_{T_0}-E_S|$, Eq. (20) simplifies to

$$\theta_F(E)\simeq CEd_A^2\frac{E-E_X^{A(0)}}{(E-E_X^{A(0)})^2+\Gamma^2}(p_{A\to B}-p_{B\to A}). \tag{21}$$

This result is surprising because the FR angle is not only determined by the probability $p_{B\to A}$ that the electron created by the pump pulse has been transferred to QD *A*. Rather, even the *sign* of the FR angle depends on the parameters δE_c (and δE_v if transfer between valence-band states is included) and $U_{A,B}$. $\theta_F\gtrless 0$ for $|\delta E_c-U_A|\gtrless|\delta E_c+U_B|$, and $\theta_F\lessgtr 0$ for $|\delta E_c-U_A|\lessgtr|\delta E_c+U_B|$. Although counterintuitive at first sight, this can be readily understood from the one- and two-exciton eigenstates. The matrix element for the virtual creation of an exciton with $s_z=1/2$, $j_z=3/2$ in QD *A* is reduced by the probability $p_{B\to A}$ that the conduction-band electron created by the pump pulse in *B* has been transferred to *A*. In this case, it blocks the creation of a second exciton with the same spin. The transition matrix element for the creation of an exciton with $s_z=-1/2$, $j_z=-3/2$ is reduced by the probability $p_{A\to B}$ that the electron with spin $s_z=-1/2$ in the conduction-band state of QD *A* is transferred to QD *B*. This transfer process is not prohibited by Pauli blocking and leads to the virtual occupation of $|B_+B_-\rangle$ which is energetically far off resonance. The interplay of both processes results in Eq. (21).

Our derivation of Eq. (21) was based on the assumption that t_c is the smallest energy scale in the system. As will be discussed in Sec. V below, for the experimental parameters in Ref. 5, $\delta E_v+U_A\simeq 0$. For $t_v=0$, this does not lead to divergencies in the perturbative expansion in t_c. However, these special parameters require that two additional two-exciton states are taken into account for the calculation of $\theta_F(E)$ because they are nearly degenerate with $|A_+B_+\rangle$, $|S\rangle$, and $|T_0\rangle$ (see Fig. 3): The states $|\tilde{S}\rangle$ and $|\tilde{T}_0\rangle$ defined in Eq. (A1) have finite overlap matrix elements with $\hat{P}_-|X_{B,+}\rangle$,

$$|\langle\tilde{T}_0|\hat{P}_-|X_{B,+}\rangle|^2=\frac{p_{B\to A}d_B^2}{2}, \tag{22a}$$

$$|\langle\tilde{S}|\hat{P}_-|X_{B,+}\rangle|^2=\frac{p_{B\to A}d_B^2}{2}. \tag{22b}$$

The spin configurations for the states $|\tilde{S}\rangle$ and $|\tilde{T}_0\rangle$ are shown schematically in Fig. 4(a). Note that both holes occupy the valence-band states of QD *B*. The accidental degeneracy of $|\tilde{S}\rangle$ and $|\tilde{T}_0\rangle$ with $|S\rangle$ and $|T_0\rangle$ arises because, for the parameters of Ref. 5, the decrease in orbital energy δE_v is comparable to the increase in Coulomb energy U_A. Transitions

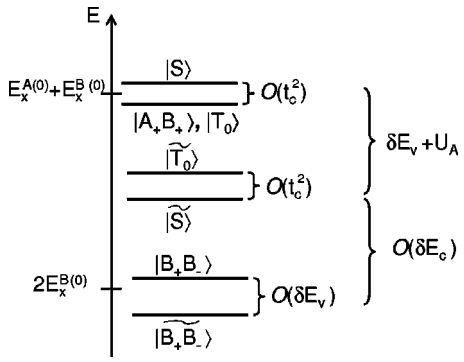

FIG. 3. Energy-level scheme of all two-exciton eigenstates discussed in the text. The eigenenergies fall into three groups which are split by terms of order $O(t_c^2)$ or $O(\delta E_v)$. For the QD's used in Ref. 5, $\delta E_v+U_A\simeq 0$, and the five states $|A_+B_+\rangle$, $|T_0\rangle$, $|S\rangle$, $|\tilde{T}_0\rangle$, and $|\tilde{S}\rangle$ are nearly degenerate.

between an initial state $|X_{B,+}\rangle$ and $|\tilde{S}\rangle$, $|\tilde{T}_0\rangle$ are two-step processes. A σ^+ polarized probe photon creates an exciton with $s_z=-1/2$ and $j_z=-3/2$ in B, and one of the conduction-band electrons in B is subsequently transferred to A. These processes are shown schematically in Fig. 4(b).

Taking into account all two-exciton states with energies $|E_i-(E_X^{A(0)}+E_X^{B(0)})|\lesssim\max[|\delta E_v+U_A|,|E_{T_0}-E_S|]$, the FR angle is

$$\theta_F(E)=\frac{CE}{2}\left\{d_A^2\left[(1-p_{B\to A})\frac{E-E_{T_0B}}{(E-E_{T_0B})^2+\Gamma^2}-(1+p_{B\to A}-2p_{A\to B})\frac{E-E_{SB}}{(E-E_{SB})^2+\Gamma^2}\right]-d_B^2 p_{B\to A}\times\left[\frac{E-E_{\tilde{T}_0B}}{(E-E_{\tilde{T}_0B})^2+\Gamma^2}+\frac{E-E_{\tilde{S}B}}{(E-E_{\tilde{S}B})^2+\Gamma^2}\right]\right\}. \quad (23)$$

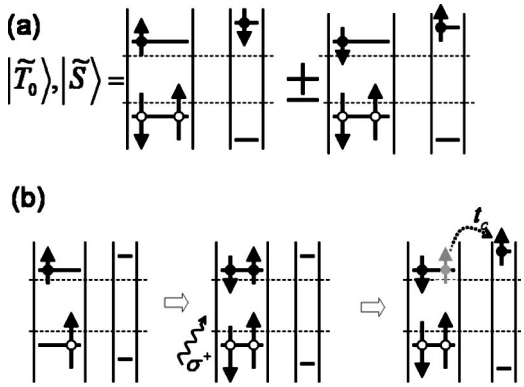

FIG. 4. (a) Schematic representation of the spin configurations for the states $|\tilde{S}\rangle$, $|\tilde{T}_0\rangle$ to leading order in t_c. (b) Transitions between an initial state $|X_{B,+}\rangle$ and $|\tilde{S}\rangle$, $|\tilde{T}_0\rangle$ are effected by the absorption of a σ^+ polarized probe photon and subsequent tunneling of one conduction-band electron.

The energy differences $E_{\tilde{T}_0B}=E_{\tilde{T}_0}-E_X^B$ and $E_{\tilde{S}B}=E_{\tilde{S}}-E_X^B$ are given by the eigenenergies in Eq. (A2). For $|E-E_{T_0B}|,|E-E_{SB}|\ll|E-E_{\tilde{T}_0B}|,|E-E_{\tilde{S}B}|$, Eq. (23) simplifies to Eq. (20).[17]

Above, we have only considered $t_c\neq 0$ and $t_v=0$, i.e., a scenario in which electrons in the valence band remain localized in the QD's while electrons in conduction-band states can be transferred. The case $t_v\neq 0$ and $t_c=0$ can be mapped onto the problem discussed above by mapping electrons onto holes, i.e., by interchanging c and v in above expressions. In particular, Eqs. (20) and (21) remain valid if the transfer probabilities for electrons are replaced by the corresponding values for holes, e.g., $p_{A\to B}=[t_v/(\delta E_v+U_A)]^2$, and the energy eigenvalues are calculated for transfer in the valence rather than the conduction band.

In the limit of small QD's with similar sizes, $U_{A,B}\gg t_{c,v}\gg\delta E_c,|\delta E_v|$, configurations in which electrons and holes occupy different QD's are strongly suppressed. If $t_{c,v}/U_{A,B}\simeq 0$ but $t_c t_v/U_{A,B}(E_X^{A(0)}-E_X^{B(0)})$ remains finite, a joint transfer of electron and hole via a virtual intermediate state is possible. Evidence for this coherent delocalization of an exciton has been reported for QD's of similar sizes.[18,19] In contrast, tunneling of excitons between a pair of QD's with different sizes is incoherent if the orbital decoherence rate is comparable to the exciton tunneling rate.[20–23]

IV. DOPING OF COUPLED QUANTUM DOTS

In the last section, we have analyzed the FR angle for an initial spin population created by optical pumping, the method used in Ref. 5. We now calculate the FR angle $\theta_F(E)$ for the case that the initial spin density is carried by an excess electron rather than an exciton. Spin injection could be achieved, e.g., by doping one CdSe QD with a single donor atom. For a chemical potential $E_c^B\lesssim\mu\lesssim E_c^A, E_c^B+U_B$, the conduction-band level of QD B is filled with one electron while QD A remains empty. The excess electron can be spin polarized by cooling in presence of a magnetic field. Again, we set $t_v=0$ to keep our results transparent.

The transfer matrix element for the conduction-band level leads to the delocalization of the excess electron in QD B,

$$|e_{B,\sigma}\rangle=\left[1+\left(\frac{t_c}{\delta E_c}\right)^2\right]^{-1/2}\left(\hat{c}_{c,\sigma}^{B\dagger}-\frac{t_c}{\delta E_c}\hat{c}_{c,\sigma}^{A\dagger}\right)|0\rangle, \quad (24)$$

with eigenenergy $E^B=E_c^B-t_c^2/\delta E_c$. Note that the energy shift is different from the one found for the exciton because there is no Coulomb attraction between electron and hole in the present case.

We calculate the FR angle for an initial state $|e_{B,+}\rangle$ and probe energy $E\simeq E_X^A$. Similar to the analysis in Sec. III, three intermediate states dominate the spectral representation for $\theta_F(E)$. These states are the following.

$$|A_+B_+^-\rangle=\hat{c}_{c,+}^{A\dagger}\hat{c}_{c,+}^{B\dagger}\hat{c}_{v,+}^{A}|0\rangle, \quad (25)$$

with energy eigenvalue

$$E_{A_+B_+^-}=E_X^{A(0)}+E_c^B \quad (26)$$

is populated by creation of an exciton with conduction and valence band spins $s_z=1/2$ and $j_z=3/2$, respectively.[24] Virtual creation of an exciton with $s_z=-1/2$ and $j_z=-3/2$ leads to transitions to the spin triplet and singlet states

$$|T_0^-\rangle=\frac{1}{\sqrt{2}}(\hat{c}^{A\dagger}_{c,-}\hat{c}^{B\dagger}_{c,+}+\hat{c}^{A\dagger}_{c,+}\hat{c}^{B\dagger}_{c,-})\hat{c}^{A}_{v,-}|0\rangle, \tag{27a}$$

$$|S^-\rangle\propto\frac{1}{\sqrt{2}}(\hat{c}^{A\dagger}_{c,-}\hat{c}^{B\dagger}_{c,+}-\hat{c}^{A\dagger}_{c,+}\hat{c}^{B\dagger}_{c,-})\hat{c}^{A}_{v,-}|0\rangle+\sqrt{2}\left(\frac{t_c}{\delta E_c}\hat{c}^{A\dagger}_{c,+}\hat{c}^{A\dagger}_{c,-}-\frac{t_c}{\delta E_c-U_A-U_B}\hat{c}^{B\dagger}_{c,+}\hat{c}^{B\dagger}_{c,-}\right)\hat{c}^{A}_{v,-}|0\rangle, \tag{27b}$$

where the normalization constant for $|S^-\rangle$ is determined by $\langle S^-|S^-\rangle=1$. The eigenenergies

$$E_{T_0^-}=E_X^{A(0)}+E_c^B, \tag{28a}$$

$$E_{S^-}=E_X^{A(0)}+E_c^B+2t_c^2\left(\frac{1}{\delta E_c-U_A-U_B}-\frac{1}{\delta E_c}\right) \tag{28b}$$

are split by the exchange coupling of the conduction-band levels. Further, there are several states with energies differing from $E_X^{A(0)}+E_c^B$ (see Appendix B). For probe pulse energies $E\simeq E_X^{A(0)}$ and $|\delta E_v+U_A-U_B|\gtrsim\Gamma$, $\theta_F(E)$ is dominated by virtual excitations into the states $|A_+B_+^-\rangle$, $|T_0^-\rangle$, and $|S^-\rangle$. In this case, all other energy eigenstates with two conduction-band electrons and one hole listed in Appendix B are energetically far off resonance and can be neglected.

The transition matrix elements of the polarization operators $\hat{P}_\pm$ between $|e_{B,+}\rangle$ and the states Eqs. (25) and (27) are readily evaluated. The probabilities for electron transfer between the QD's are now given by

$$p^-_{B\to A}=\left(\frac{t_c}{\delta E_c}\right)^2, \tag{29a}$$

$$p^-_{A\to B}=\left(\frac{t_c}{\delta E_c-U_A-U_B}\right)^2. \tag{29b}$$

Then,

$$|\langle A_+B_+^-|\hat{P}_+|e_{B,+}\rangle|^2=(1-p^-_{B\to A})d_A^2, \tag{30a}$$

$$|\langle T_0^-|\hat{P}_-|e_{B,+}\rangle|^2=\frac{1-p^-_{B\to A}}{2}d_A^2, \tag{30b}$$

$$|\langle S^-|\hat{P}_-|e_{B,+}\rangle|^2=\frac{1+p^-_{B\to A}-2p^-_{A\to B}}{2}d_A^2. \tag{30c}$$

Inserting these matrix elements into the spectral representation of $\theta_F(E)$, Eq. (6), we find for the FR angle

$$\theta_F(E)=\frac{CEd_A^2}{2}\left[(1-p^-_{B\to A})\frac{E-E^-_{T_0B}}{(E-E^-_{T_0B})^2+\Gamma^2}-(1+p^-_{B\to A}-2p^-_{A\to B})\frac{E-E^-_{SB}}{(E-E^-_{SB})^2+\Gamma^2}\right] \tag{31}$$

for probe energies $E\simeq E_X^{A(0)}$, in close analogy to Eq. (20) for optical spin injection. The energy differences are defined by $E^-_{T_0B}=E_{T_0^-}-E^B$ and $E^-_{SB}=E_{S^-}-E^B$. Because of the exchange splitting between $|T_0^-\rangle$ and $|S^-\rangle$, $\theta_F(E)$ will in general exhibit several peaks and lack point-inversion symmetry. The functional dependence on probe energy is determined by the transfer probabilities and the energy differences $E^-_{T_0B}$ and E^-_{SB}. For a more detailed analysis which takes into account all finite transition matrix elements up to $\mathcal{O}(t_c^2)$, see Appendix B.

Experiments on doped QD's could provide valuable information supplementing the experimental data obtained for optical pumping. The main advantage over optical spin injection is that spin decoherence times are expected to be substantially longer because they are not limited by electron-hole recombination. Even more importantly, FR measurements on doped coupled QD's can clarify whether spin transfer occurs predominantly between the conduction- or valence-band levels because, for $t_c=0$ and $t_v\neq 0$, $\theta_F(E)\simeq 0$ for probe energies $E\simeq E_X^{A(0)}$.

V. COMPARISON WITH EXPERIMENT

In order to compare the results of Sec. III with experimental data from Ref. 5, we first provide numerical values for δE_c, δE_v, U_A, and U_B. The energy-level spectrum of CdSe QD's is well established both experimentally and theoretically.[25,26] The absorption energies $E_X^{A(0)}=2.41$ eV and $E_X^{B(0)}=2.06$ eV in Ref. 5 are consistent with $r_A\simeq 2.0$ nm and $r_B\simeq 3.5$ nm, and we will use these radii for the following calculations. From Ref. 25, $\delta E_c\simeq 0.30$ eV and $\delta E_v\simeq -0.10$ eV.

From the bulk values for the static dielectric constant, $\epsilon=9.7$, and the band masses in the conduction and valence band, $m_c/m_e=0.12$ and $m_v/m_e=0.45$, one obtains the exciton radius 5.4 nm.[27–29,7] The exciton radius is larger than $r_{A,B}$, and electrons and holes are strongly confined in the QD's as assumed in Eq. (1). The characteristic energy scale of the Coulomb interaction is $U_\nu\simeq e^2/4\pi\epsilon\epsilon_0 r_\nu$. For the given values of r_A and r_B, $U_A=0.07$ eV and $U_B=0.04$ eV.

The Hamiltonian Eq. (1) does not take into account biexciton shifts, the exciton fine structure, and interdot Coulomb interactions. For CdSe QD's with radii 1.5–4 nm, the biexciton shift is of order 0.01–0.02 eV (Ref. 30) and the characteristic energy splitting between bright and dark excitons is smaller than 0.01 eV.[31] The characteristic energy scale for interdot Coulomb interactions is $U_{AB}\simeq e^2/4\pi\epsilon_0\epsilon(r_A+r_B)\leqslant 0.03$ eV. However, it is relevant only if neither of the two QD's is electrically neutral. The most important effect of the interdot Coulomb interaction is to lower the energy eigenval-

ues of $|\tilde{T}_0\rangle$ and $|\tilde{S}\rangle$ [Eq. (A1)] by U_{AB}. All these energy scales are small compared to the level broadening Γ and can safely be neglected.

In the following, we assume that only electrons in conduction-band levels are transferred between the QD's while valence-band electrons remain localized. As discussed in Sec. IV, this assumption can be tested by experiments on doped QD's. Mediated by electron transfer through the molecular bridge, the lowest conduction-band level in QD *B* hybridizes with the lowest conduction-band level in QD *A*. Comparing the observed energy shift $E_X^B - E_X^{B(0)} = -0.02\,\mathrm{eV}$ with Eq. (11), we find

$$t_c = \sqrt{(E_X^{B(0)} - E_X^B)(\delta E_c + U_B)} = 0.082\,\mathrm{eV}. \tag{32}$$

Our theory predicts that the exciton absorption peak for QD *A* is shifted to larger energies for the coupled QD's, in contrast to the experimental result $E_X^A - E_X^{A(0)} < 0$. The most likely explanation for this is that the lowest conduction-band level in QD *A* hybridizes also with higher excited levels in QD *B* which are nearly degenerate with E_c^A.[32] In order to account for quantitative changes effected by this hybridization, the energy $E_X^{A(0)}$ must be replaced by the true value of the hybridized state in all expressions for the two-exciton eigenenergies. This value can be obtained from $E_X^{A(0)} + t_c^2/(\delta E_c + U_A) \simeq 2.36\,\mathrm{eV}$, where the latter is the experimental value for the exciton absorption edge of QD *A* in the coupled QD's. Hence, $E_X^{A(0)} \to 2.33\,\mathrm{eV}$.

From these parameters, we calculate for the transfer probabilities between the lowest conduction-band states $p_{A\to B} = 0.13$ and $p_{B\to A} = 0.06$. The energy differences between the two-exciton states and the initial state are $E_{T_0 B} = 2.35\,\mathrm{eV}$, $E_{SB} = 2.37\,\mathrm{eV}$, $E_{\tilde{T}_0 B} = 2.32\,\mathrm{eV}$, $E_{\tilde{S}B} = 2.31\,\mathrm{eV}$. The oscillator strength for exciton creation, proportional to $d_{A,B}^2$, is independent of the QD size in the strong confinement regime and proportional to the QD volume for weak confinement. Because both QD's are close to the strong confinement limit, we assume a weak scaling $d_B^2/d_A^2 = 2$ for the following figures.

In Fig. 5(a), we show the FR angle calculated from Eq. (21) as a function of probe energy for different values of Γ, $\Gamma = 0.05\,\mathrm{eV}$ (solid), $0.02\,\mathrm{eV}$ (dashed), and $0.08\,\mathrm{eV}$ (dotted). We note that even qualitative features depend strongly on the microscopic parameters such as Γ. For small Γ, additional peaks emerge because the contributions from the individual two-exciton states can be resolved.

In spite of the dependence on microscopic parameters, some pronounced features in $\theta_F(E)$ are generally present: (i) $\theta_F(E)$ does not exhibit point-inversion symmetry, in stark contrast to the FR angle expected from virtual transitions to a single state. (ii) θ_F has in general more than two maxima or minima. The positions and heights of the extrema are determined by the interplay of the transfer probabilities $p_{A\to B}$ and $p_{B\to A}$, and the energy splittings between the different two-exciton states. Experiments have demonstrated the strong dependence of the FR angle on the probe energy *E*, including a fine structure of the resonance.[33]

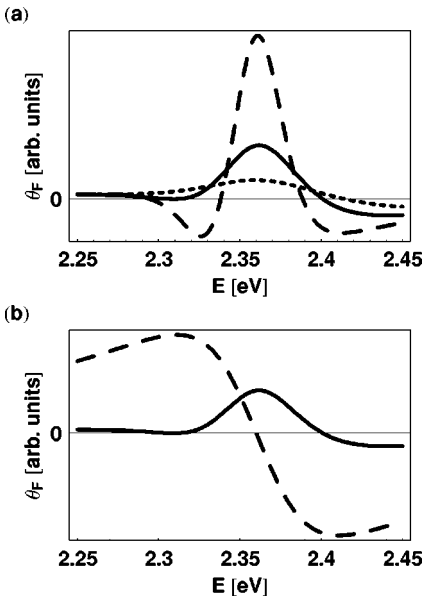

FIG. 5. (a) Plot of the FR angle as a function of probe pulse frequency calculated from Eq. (21) for different level broadenings $\Gamma = 0.05\,\mathrm{eV}$ (solid), $0.02\,\mathrm{eV}$ (dashed), and $0.08\,\mathrm{eV}$ (dotted). All other parameters are as described in the text. For small Γ, $\theta_F(E)$ clearly shows the individual contributions from the various two-exciton states. (b) Comparison of the FR angle for coupled QD's for $\Gamma = 0.05\,\mathrm{eV}$ (solid) with the calculated signal for a *AA* structure (dashed).

In Fig. 5(b), we compare the calculated FR signal for coupled QD's *A* and *B* with the corresponding result for uncoupled QD's *A* pumped at resonance. For a probe energy $E \simeq 2.42\,\mathrm{eV}$, the FR signal for coupled QD's *A* and *B* is significantly smaller than the FR signal of the *AA* system, consistent with experimental observations.[5]

Note that in Fig. 5 we show the FR angle in arbitrary units because its absolute numerical value depends sensitively on unknown experimental parameters such as the packing density of QD's and the number of QD's *A* which are coupled to at least one QD *B*. For a spin transfer probability $p_{B\to A} = 10\%$, assuming close packing of the QD's and that every QD *A* is coupled to one QD *B*, we estimate the maximum value of the Faraday rotation angle to be 0.02 rad for an *ABAABA*-structure as investigated in Ref. 5.

So far, we have assumed that the symmetry axis of the CdSe QD's with hexagonal crystal structure is parallel to the propagation direction of pump and probe laser pulses. However, in experiment the QD's are randomly oriented. We discuss next how the random orientation changes our results. The propagation direction of pump and probe laser pulse is $\hat{\mathbf{z}}$, the polarization vector of the probe pulse $\hat{\mathbf{x}}$, and the symmetry axes of QD's *A* and *B* are denoted by $\hat{\mathbf{c}}_A$ and $\hat{\mathbf{c}}_B$, respectively. We define the azimuthal angles $\phi_A = \angle(\hat{\mathbf{x}}, \hat{\mathbf{c}}_A)$ and $\phi_B = \angle(\hat{\mathbf{x}}, \hat{\mathbf{c}}_B)$, and the angle enclosed by the two symmetry axes $\phi_{AB} = \angle(\hat{\mathbf{c}}_A, \hat{\mathbf{c}}_B)$ [see Fig. 6(a)]. The conduction-band spin eigenstates with quantization axis $\hat{\mathbf{c}}_{A,B}$ are denoted by $|\uparrow_{A,B}\rangle$ and $|\downarrow_{A,B}\rangle$.

For arbitrary angle $\angle(\hat{\mathbf{z}}, \hat{\mathbf{c}}_B)$, the probability for the circu-

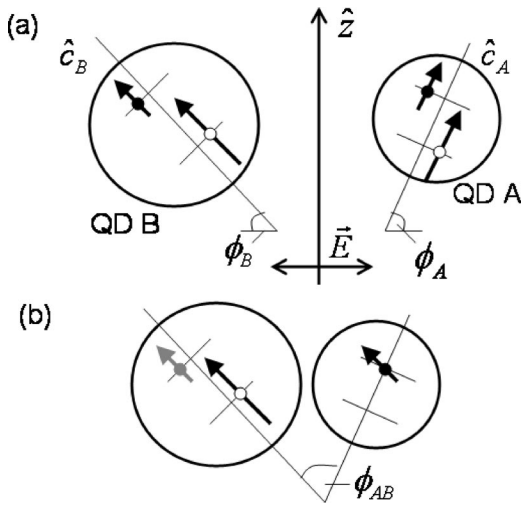

FIG. 6. (a) The hexagonal symmetry axes of QD's *A* and *B* are in general oriented randomly relative to the direction of the laser pump and probe pulse. Because of the interband selection rules, a σ^- circularly polarized laser pulse generates a spin polarization along the symmetry axis of the respective QD. (b) A conduction-band electron created in QD *B* retains its spin direction on transfer to QD *A*. FR in QD *A* probes the projection of this spin onto the symmetry axis $\hat{\mathbf{c}}_A$, which gives rise to a factor $\cos\phi_{AB}$ for the first and second term in Eq. (33).

larly polarized pump pulse to create a net spin polarization in the conduction-band level decreases from its maximum value at $\angle(\hat{\mathbf{z}},\hat{\mathbf{c}}_B)=0$ to zero at $\angle(\hat{\mathbf{z}},\hat{\mathbf{c}}_B)=\pi/2$. For $\angle(\hat{\mathbf{z}},\hat{\mathbf{c}}_B)<\pi/2$, the majority of conduction-band electrons is in spin state $|\uparrow_B\rangle$, with the quantization axis defined by $\hat{\mathbf{c}}_B$. On transfer to QD *A*, the conduction-band electron retains its spin state because states with $s_z=\pm 1/2$ are degenerate in both QD's and t_c is spin-independent. The characteristic level spacing of valence-band states is large compared to the crystal-field splitting in bulk CdSe, which allows us to treat the latter as a small perturbation, following Ref. 30.

In the following, we calculate the FR angle for a random orientation of QD's assuming that the pump pulse has created a conduction-band electron with spin $|\uparrow_B\rangle$. The random orientation of QD's affects the FR of the probe pulse in two ways. First, the matrix elements for transitions from the $j_z=\pm 3/2$ valence-band levels to the $s_z=\pm 1/2$ conduction-band levels in QD *A* (*B*) decrease by $\sin\phi_A$ ($\sin\phi_B$) compared to the oriented sample.[30] More importantly, also the relative orientation of $\hat{\mathbf{c}}_A$ and $\hat{\mathbf{c}}_B$ modifies the FR angle. For illustration, consider two QD's with $t_c=0$, and a conduction-band electron in spin state $|\uparrow_B\rangle$ in *B*. The σ^- circularly polarized component of the probe pulse with $E\simeq E_X^A$ excites a virtual exciton in *A*, with a conduction-band electron in spin state $|\uparrow_A\rangle$. Note that the spin direction is defined by $\hat{\mathbf{c}}_A$, the symmetry axis of *A*. Expanding $|\uparrow_A\rangle=\cos(\phi_{AB}/2)|\uparrow_B\rangle+i\sin(\phi_{AB}/2)|\downarrow_B\rangle$ in terms of the eigenstates along quantization axis $\hat{\mathbf{c}}_B$, the product state of the two excitons contains terms in which the two conduction-band spins are antiparallel and have a finite overlap with the spin singlet state. This is in stark contrast to the oriented sample, where the two conduction-band electrons would always form a triplet.

The analogous analysis for coupled QD's must take into account both the reduced transition matrix elements for the probe pulse and the relative orientation of QD's *A* and *B*. Because virtual transitions to $|\tilde{T}_0\rangle$ and $|\tilde{S}\rangle$ involve excitation of QD *B* which was populated by the pump pulse, the matrix elements in Eq. (22) are reduced by a factor $|\sin\phi_B|$ which is independent of the relative orientation of $\hat{\mathbf{c}}_A$ and $\hat{\mathbf{c}}_B$. In contrast, virtual transitions in QD *A* probe the spin polarization relative to the quantization axis $\hat{\mathbf{c}}_A$ after an electron with spin pointing along $\hat{\mathbf{c}}_B$ has been transferred, and the transition matrix elements depend also on ϕ_{AB} [Fig. 6(b)]. For the FR angle, we find

$$\theta_F(E)=\frac{CE}{2}\left\{d_A^2\cos\phi_{AB}\sin^2\phi_A\left[(1-p_{B\to A})\times\frac{E-E_{T_0B}}{(E-E_{T_0B})^2+\Gamma^2}-(1+p_{B\to A}-2p_{A\to B})\times\frac{E-E_{SB}}{(E-E_{SB})^2+\Gamma^2}\right]-d_B^2\sin^2\phi_B\,p_{B\to A}\times\left[\frac{E-E_{\tilde{T}_0B}}{(E-E_{\tilde{T}_0B})^2+\Gamma^2}+\frac{E-E_{\tilde{S}B}}{(E-E_{\tilde{S}B})^2+\Gamma^2}\right]\right\}. \tag{33}$$

The dependence on the relative orientation of the two QD's, ϕ_{AB}, is readily understood. For $\phi_{AB}=\pi/2$, the first and second term in the expression for $\theta_F(E)$ vanish because the conduction-band spin created in QD *B* is perpendicular to the spin quantization axis in QD *A*. A laser pulse probing QD *A* does not show any FR because the net spin along $\hat{\mathbf{c}}_A$ vanishes [Fig. 6(b)].

In experiment, $\hat{\mathbf{c}}_A$ and $\hat{\mathbf{c}}_B$ are randomly distributed over the unit sphere. Performing this average in Eq. (33), we find for the FR angle

$$\overline{\theta_F}(E)=\frac{CE}{2}\left\{\frac{3}{16}d_A^2\left[(1-p_{B\to A})\frac{E-E_{T_0B}}{(E-E_{T_0B})^2+\Gamma^2}-(1+p_{B\to A}-2p_{A\to B})\frac{E-E_{SB}}{(E-E_{SB})^2+\Gamma^2}\right]-\frac{2}{3}d_B^2p_{B\to A}\left[\frac{E-E_{\tilde{T}_0B}}{(E-E_{\tilde{T}_0B})^2+\Gamma^2}+\frac{E-E_{\tilde{S}B}}{(E-E_{\tilde{S}B})^2+\Gamma^2}\right]\right\}. \tag{34}$$

Note that the spectral weight of the last term increases compared to the oriented sample.

VI. CONCLUSION

We have calculated the Faraday rotation angle for coupled QD's as a function of the probe pulse frequency. We have considered an initial spin polarization in neutral QD's (created by optical pumping) and of one excess electron in the two coupled QD's. Our results lead us to the following conclusions.

(i) The Faraday rotation angle shows a nontrivial functional dependence on the probe energy, the details of which depend on the spin-exchange energy and spin transfer probabilities [see Eq. (21) and Fig. 5(a)]. Most notably, because several two-exciton states are separated in energy by a small spin-exchange coupling, $\theta_F(E)$ is not invariant under point-inversion symmetry. Measurement of $\theta_F(E)$ as a function of probe energy would allow one to identify the contributions of the various two-exciton states that are virtually excited by the probe pulse.

(ii) Experiments on doped QD's would allow one to determine whether spin transfer is mediated by transfer in the conduction- or valence-band states. In particular, from a vanishing Faraday rotation angle for probe pulse energies close to the resonance of QD A one could exclude that an excess electron injected into QD B has been transferred to A. In contrast, for optical spin injection, spin could be transferred both between conduction- and valence-band states.

(iii) In general, measurement of the Faraday rotation signal at a given probe frequency does not provide enough information to determine spin transfer probabilities between the QD's. However, from the experimentally observed energy shifts, we calculate a characteristic energy scale $t_c = 0.08$ eV for spin transfer in the conduction band. Based on the transfer Hamiltonian ansatz, this implies a probability of 6% for electron spin to be transferred from QD B to QD A, and of 13% for the opposite direction.

The purpose of this work was to establish the connection between spin transfer and the Faraday rotation signal observed in experiment. Our analysis was based on a transfer Hamiltonian ansatz. Some of the most interesting results of Ref. 5 remain to be explored theoretically. Most notably, the transfer Hamiltonian ansatz is based on the assumption that electrons are transferred between the QD's via the bridging benzene molecule. Microscopic work will have to clarify why conjugated molecules provide efficient transfer paths between QD's.

The results obtained here can provide important guidance also for the identification of microscopic transfer mechanisms. The increase of the Faraday rotation signal at a fixed probe frequency has been interpreted as increase of the spin transfer efficiency for higher temperatures.[5] According to our results, an increase in the transfer matrix element t_c also leads to a shift of the exciton edge in absorption spectra toward lower energies. If the exciton absorption edge does not change with increasing temperature, the increased Faraday rotation signal is more likely effected, e.g., by additional incoherent transfer paths than by an increase of the transfer matrix element.

ACKNOWLEDGMENTS

We gratefully acknowledge helpful discussion with W. Lau, A. Holleitner, and, in particular, M. Ouyang. This work was supported by DARPA, ONR, the EU TMR network MOLNANOMAG Grant No. HPRN-CT-1999-00012, the Swiss NCCR Nanoscience, and the Swiss NSF.

APPENDIX A: TWO-EXCITON EIGENSTATES OF COUPLED QUANTUM DOTS

In order to evaluate the FR angle $\theta_F(E)$ from Eq. (6) for arbitrary probe energies E, all two-exciton intermediate states $|\psi_i\rangle$ with finite transition matrix elements $\langle\psi_i|\hat{P}_{\pm}|X_{B,+}\rangle$ must be calculated. States with energies $E_i \simeq E + E_X^{B(0)}$ lead to the dominant contributions in the expression for the FR angle, Eq. (6). The states $|A_+B_+\rangle$, $|S\rangle$, and $|T_0\rangle$ defined in Eqs. (12) and (14) have energy eigenvalues E_i with $|E_X^{A(0)} + E_X^{B(0)} - E_i| \leq \mathcal{O}[t_c^2/(\delta E_c - U_A), t_c^2/(\delta E_c + U_A)]$, and are the most important intermediate states for probe pulse energies $E \simeq E_X^{A(0)}$. However, for the experimental values of Ref. 5, $\delta E_v + U_A$ is small and two additional two-exciton states must be taken into account.

The states

$$|\tilde{T}_0\rangle = \frac{1}{\sqrt{2}}(\hat{c}^{A\dagger}_{c,-}\hat{c}^{B\dagger}_{c,+} + \hat{c}^{A\dagger}_{c,+}\hat{c}^{B\dagger}_{c,-})\hat{c}^{B}_{v,+}\hat{c}^{B}_{v,-}|0\rangle, \quad \text{(A1a)}$$

$$\begin{aligned}|\tilde{S}\rangle \propto{}& \frac{1}{\sqrt{2}}(\hat{c}^{A\dagger}_{c,-}\hat{c}^{B\dagger}_{c,+} - \hat{c}^{A\dagger}_{c,+}\hat{c}^{B\dagger}_{c,-})\hat{c}^{B}_{v,+}\hat{c}^{B}_{v,-}|0\rangle \\ &+ \sqrt{2}\left(\frac{t_c}{\delta E_c + U_A + 2U_B}\hat{c}^{A\dagger}_{c,+}\hat{c}^{A\dagger}_{c,-}\right. \\ &\left. - \frac{t_c}{\delta E_c + U_B}\hat{c}^{B\dagger}_{c,+}\hat{c}^{B\dagger}_{c,-}\right)\hat{c}^{B}_{v,+}\hat{c}^{B}_{v,-}|0\rangle \end{aligned} \quad \text{(A1b)}$$

differ from the corresponding states in Eq. (14) in that both holes are localized in QD B. The normalization constant for $|\tilde{S}\rangle$ is fixed by $\langle\tilde{S}|\tilde{S}\rangle = 1$. The eigenenergies

$$E_{\tilde{T}_0} = E_X^{A(0)} + E_X^{B(0)} + \delta E_v + U_A, \quad \text{(A2a)}$$

TABLE I. Two-exciton eigenstates $|\psi_i\rangle$ which contribute to the FR angle up to second order in t_c. We also list the corresponding eigenenergies to $O(t_c^0)$ and evaluate them for the parameters discussed in Sec. V. As noted in the main text, the degeneracy of $|\tilde{T}_0\rangle$, $|\tilde{S}\rangle$ with $|T_0\rangle$, $|S\rangle$ is a consequence of $\delta E_v + U_A \simeq 0$ for the QD's used in experiment.

$\|\psi_i\rangle$	E_i	$E_i - E_X^B$ [eV]
$\|A_+B_+\rangle$	$E_X^{A(0)} + E_X^{B(0)}$	2.35
$\|T_0\rangle$	$E_X^{A(0)} + E_X^{B(0)}$	2.35
$\|S\rangle$	$E_X^{A(0)} + E_X^{B(0)}$	2.37
$\|B_+B_-\rangle$	$E_c^B - E_v^A + E_X^{B(0)}$	2.06
$\|\tilde{T}_0\rangle$	$E_c^A - E_v^B + E_X^{B(0)}$	2.32
$\|\tilde{S}\rangle$	$E_c^A - E_v^B + E_X^{B(0)}$	2.33
$\widetilde{\|B_+B_-\rangle}$	$2E_X^{B(0)}$	2.04

$$E_{\tilde{S}}=E_X^{A(0)}+E_X^{B(0)}+\delta E_v+U_A + 2t_c^2\left(\frac{1}{\delta E_c+U_B}-\frac{1}{\delta E_c+2U_B+U_A}\right) \quad \text{(A2b)}$$

are shifted relative to E_{T_0} and E_S by δE_v+U_A.

The state

$$|\widetilde{B_+B_-}\rangle\propto\left[\hat{c}_{c,+}^{B\dagger}\hat{c}_{c,-}^{B\dagger}+\frac{t_c}{\delta E_c+U_B}(\hat{c}_{c,-}^{A\dagger}\hat{c}_{c,+}^{B\dagger}-\hat{c}_{c,+}^{A\dagger}\hat{c}_{c,-}^{B\dagger}) + \frac{2t_c^2\hat{c}_{c,+}^{A\dagger}\hat{c}_{c,-}^{A\dagger}}{(\delta E_c+U_B)(2\delta E_c+U_A+3U_B)}\right]\hat{c}_{v,+}^{B}\hat{c}_{v,-}^{B}|0\rangle, \quad \text{(A3)}$$

with

$$E_{\widetilde{B_+B_-}}=2E_X^{B(0)}-2\frac{t_c^2}{\delta E_c+U_B} \quad \text{(A4)}$$

is energetically separated from E_{T_0} and E_S by $E_X^{A(0)}-E_X^{B(0)}$.

In Table I, we summarize all two-exciton eigenstates which contribute to the spectral representation of $\theta_F(E)$ up to order t_c^2. We also list the formal expressions for their eigenenergies to leading order $O(t_c^0)$ and give the numerical values, taking into account terms up to $O(t_c^2)$ for the parameters discussed in Sec. V.

APPENDIX B: EIGENSTATES OF DOPED COUPLED QUANTUM DOTS

Here, we calculate eigenstates and energy eigenvalues for states with two electrons and one hole in the coupled QD's. These are the intermediate states $|\psi_i\rangle$ in Eq. (6) which have finite overlap matrix elements with $\hat{P}_{\pm}|e_{B,+}\rangle$ and determine the FR angle for coupled QD's doped with a single excess electron.

In addition to the states $|A_+B_+^-\rangle$, $|S^-\rangle$, and $|T_0^-\rangle$ defined in Eqs. (25) and (27), five states have contributions of order t_c^2 to the FR angle. These are

$$|B_+B_-^-\rangle\propto\left[\hat{c}_{c,+}^{B\dagger}\hat{c}_{c,-}^{B\dagger}+\frac{t_c}{\delta E_c-U_A-U_B}(\hat{c}_{c,-}^{A\dagger}\hat{c}_{c,+}^{B\dagger} - \hat{c}_{c,+}^{A\dagger}\hat{c}_{c,-}^{B\dagger})\right]\hat{c}_{v,-}^{A}|0\rangle, \quad \text{(B1a)}$$

$$|\widetilde{A_+B_+}^-\rangle=\hat{c}_{c,+}^{A\dagger}\hat{c}_{c,+}^{B\dagger}\hat{c}_{v,+}^{B}|0\rangle, \quad \text{(B1b)}$$

$$|\tilde{T}_0^-\rangle=\frac{1}{\sqrt{2}}(\hat{c}_{c,-}^{A\dagger}\hat{c}_{c,+}^{B\dagger}+\hat{c}_{c,+}^{A\dagger}\hat{c}_{c,-}^{B\dagger})\hat{c}_{v,-}^{B}|0\rangle, \quad \text{(B1c)}$$

$$|\tilde{S}^-\rangle\propto\left[\frac{1}{\sqrt{2}}(\hat{c}_{c,-}^{A\dagger}\hat{c}_{c,+}^{B\dagger}-\hat{c}_{c,+}^{A\dagger}\hat{c}_{c,-}^{B\dagger}) + \sqrt{2}\left(\frac{t_c}{\delta E_c+U_A+U_B}\hat{c}_{c,+}^{A\dagger}\hat{c}_{c,-}^{A\dagger} - \frac{t_c}{\delta E_c}\hat{c}_{c,+}^{B\dagger}\hat{c}_{c,-}^{B\dagger}\right)\right]\hat{c}_{v,-}^{B}|0\rangle, \quad \text{(B1d)}$$

$$\widetilde{B_+B_-}^-\rangle\propto\left[\hat{c}_{c,+}^{B\dagger}\hat{c}_{c,-}^{B\dagger}+\frac{t_c}{\delta E_c}(\hat{c}_{c,-}^{A\dagger}\hat{c}_{c,+}^{B\dagger}-\hat{c}_{c,+}^{A\dagger}\hat{c}_{c,-}^{B\dagger})\right]\hat{c}_{v,-}^{B}|0\rangle, \quad \text{(B1e)}$$

with the proportionality constants chosen to ensure normalization. The corresponding energy eigenvalues are

$$E_{B_+B_-^-}=2E_c^B+U_B-E_v^A-2\frac{t_c^2}{\delta E_c-U_A-U_B}, \quad \text{(B2a)}$$

$$E_{\widetilde{A_+B_+}^-}=E_X^{B(0)}+E_c^A, \quad \text{(B2b)}$$

$$E_{\tilde{T}_0^-}=E_X^{B(0)}+E_c^A, \quad \text{(B2c)}$$

$$E_{\tilde{S}^-}=E_X^{B(0)}+E_c^A + 2t_c^2\left(\frac{1}{\delta E_c}-\frac{1}{\delta E_c+U_A+U_B}\right), \quad \text{(B2d)}$$

$$E_{\widetilde{B_+B_-}^-}=E_X^{B(0)}+E_c^B-2\frac{t_c^2}{\delta E_c}. \quad \text{(B2e)}$$

From Eq. (B1), we obtain the transition matrix elements in terms of the transfer probabilities defined in Eq. (29),

$$|\langle B_+B_-^-|\hat{P}_-|e_{B,+}\rangle|^2=p_{A\to B}^- d_A^2, \quad \text{(B3a)}$$

$$|\langle\widetilde{A_+B_+}^-|\hat{P}_+|e_{B,+}\rangle|^2=p_{B\to A}^- d_B^2, \quad \text{(B3b)}$$

$$|\langle\tilde{T}_0^-|\hat{P}_-|e_{B,+}\rangle|^2=\frac{p_{B\to A}^-}{2}d_B^2, \quad \text{(B3c)}$$

TABLE II. Eigenstates $|\psi_i\rangle$ with two electrons and one hole which contribute to the FR angle up to second order in t_c. We also list the corresponding eigenenergies to $O(t_c^0)$ and evaluate them for the parameters discussed in Sec. V.

$\|\psi_i\rangle$	E_i	$E_i-E_c^B$ [eV]
$\|A_+B_+^-\rangle$	$E_X^{A(0)}+E_c^B$	2.34
$\|T_0^-\rangle$	$E_X^{A(0)}+E_c^B$	2.34
$\|S^-\rangle$	$E_X^{A(0)}+E_c^B$	2.36
$\|B_+B_-^-\rangle$	$2E_c^B+U_B-E_v^A$	2.19
$\|\widetilde{A_+B_-}^-\rangle$	$E_X^{B(0)}+E_c^A$	2.27
$\|\tilde{T}_0^-\rangle$	$E_X^{B(0)}+E_c^A$	2.27
$\|\tilde{S}^-\rangle$	$E_X^{B(0)}+E_c^A$	2.28
$\|\widetilde{B_+B_-}^-\rangle$	$E_X^{B(0)}+E_c^B$	2.03

$$|\langle \tilde{S}^- | \hat{P}_- | e_{B,+} \rangle|^2 = \frac{p^-_{B\to A}}{2} d_B^2, \tag{B3d}$$

$$|\langle \widetilde{B_+ B_-}^- | \hat{P}_- | e_{B,+} \rangle|^2 = (1 - p^-_{B\to A}) d_B^2. \tag{B3e}$$

These transition matrix elements and the eigenenergies allow one to calculate $\theta_F(E)$ for arbitrary energies. However, the states in Eq. (B1) are offset in energy from $E_X^{A(0)} + E^B$. For probe energies $E \simeq E_X^{A(0)}$, virtual transitions to the states $|A_+ B_+^-\rangle$, $|S^-\rangle$, and $|T_0^-\rangle$ are dominant, and $\theta_F(E)$ simplifies to the approximate expression given in Eq. (31).

In Table II, we list all states with two electrons and one hole which contribute to $\theta_F(E)$ up to $O(t_c^2)$. We also provide the general expressions for the eigenenergies to order $O(t_c^0)$ and evaluate them numerically for the parameters discussed in Sec. V.

*Electronic address: florian@iquest.ucsb.edu

[1] S.A. Wolf, D.D. Awschalom, R.A. Buhrman, J.M. Daughton, S. von Molnár, M.L. Roukes, A.Y. Chtchelkanova, and D.M. Treger, Science **294**, 1488 (2001).

[2] *Semiconductor Spintronics and Quantum Computation*, edited by D.D. Awschalom, D. Loss, and N. Samarth (Springer, Berlin, 2002).

[3] J.M. Kikkawa, I.P. Smorchkova, N. Samarth, and D.D. Awschalom, Science **277**, 1284 (1997).

[4] D. Loss and D.P. DiVincenzo, Phys. Rev. A **57**, 120 (1998).

[5] M. Ouyang and D.D. Awschalom, Science **301**, 1074 (2003).

[6] Note that a Förster process, as discussed, e.g., by A.O. Govorov, Phys. Rev. B **68**, 075315 (2003), cannot explain the result of Ref. 5, where spin is transferred from the larger to the smaller QD.

[7] H. Fu, L.-W. Wang, and A. Zunger, Phys. Rev. B **59**, 5568 (1999).

[8] A.L. Efros, Phys. Rev. B **46**, 7448 (1992).

[9] J.A. Gupta, D.D. Awschalom, A.L. Efros, and A.V. Rodina, Phys. Rev. B **66**, 125307 (2002).

[10] A.V. Rodina, A.L. Efros, and A.Y. Alekseev, Phys. Rev. B **67**, 155312 (2003).

[11] J. Schrier and K.B. Whaley, Phys. Rev. B **67**, 235301 (2003).

[12] S. Hugonnard-Bruyère, C. Buss, F. Vouilloz, R. Frey, and C. Flytzanis, Phys. Rev. B **50**, 2200 (1994).

[13] N. Linder and L.J. Sham, Physica E (Amsterdam) **2**, 412 (1998).

[14] L.J. Sham, J. Magn. Magn. Mater. **200**, 219 (1999).

[15] Two-exciton eigenstates which are energetically offset compared to $E + E_X^B$ will also contribute to the FR signal. However, their contribution varies slowly as a function of probe energy and leads at most to an offset in the results derived below. See also Appendix A.

[16] O. Gywat, G. Burkard, and D. Loss, Phys. Rev. B **65**, 205329 (2002).

[17] In order to calculate $\theta_F(E)$ for arbitrary energies E, also virtual transitions to $|B_+ B_-\rangle$, $|\widehat{B_+ B_-}\rangle$, and the vacuum state $|0\rangle$ have to be taken into account. The corresponding expression is omitted here, but can be directly obtained from Eq. (6).

[18] G. Schedelbeck, W. Wegscheider, M. Bichler, and G. Abstreiter, Science **278**, 1792 (1997).

[19] M. Bayer, P. Hawrylak, K. Hinzer, S. Fafard, M. Korkusinski, Z.R. Wasilewski, O. Stern, and A. Forchel, Science **291**, 451 (2001).

[20] R. Heitz, I. Mukhametzhanov, P. Chen, and A. Madhukar, Phys. Rev. B **58**, 10 151 (1998).

[21] A. Tackeuchi, T. Kuroda, K. Mase, Y. Nakata, and N. Yokoyama, Phys. Rev. B **62**, 1568 (2000).

[22] H.D. Robinson, B.B. Goldberg, and J.L. Merz, Phys. Rev. B **64**, 075308 (2001).

[23] J. Seufert, M. Obert, G. Bacher, A. Forchel, T. Passow, K. Leonardi, and D. Hommel, Phys. Rev. B **64**, 121303 (2001).

[24] The superscript distinguishes the states with two electrons and one hole from the two-exciton states discussed in Sec. III.

[25] A.I. Ekimov, F. Hache, M.C. Schanne-Klein, D. Ricard, C. Flytzanis, I.A. Kudryavtsev, T.V. Yazeva, A.V. Rodina, and A.L. Efros, J. Opt. Soc. Am. B **10**, 100 (1993).

[26] D.J. Norris, A. Sacra, C.B. Murray, and M.G. Bawendi, Phys. Rev. Lett. **72**, 2612 (1994).

[27] R.R. Reeber, J. Mater. Sci. **11**, 590 (1976).

[28] R.G. Wheeler and J.O. Dimmock, Phys. Rev. **125**, 1805 (1962).

[29] R. Geick, C.H. Perry, and S.S. Mitra, J. Appl. Phys. **37**, 1994 (1966).

[30] A.L. Efros, M. Rosen, M. Kuno, M. Nirmal, D.J. Norris, and M. Bawendi, Phys. Rev. B **54**, 4843 (1996).

[31] M. Achermann, J.A. Hollingsworth, and V.I. Klimov, Phys. Rev. B **68**, 245302 (2003).

[32] This hybridization with higher lying levels in QD B does not invalidate our calculation of the FR angle in Sec. III because the pump pulse leads to occupation of the lowest conduction-band level in QD B only.

[33] M. Ouyang (private communication).